

基于偶极子方环交叉元有损电容表面的薄宽带吸波器设计

林一夫^{1,2}, 杨贤昭^{1*}, 李享成^{2**}

¹武汉科技大学冶金自动化与检测技术教育部工程研究中心, 湖北 武汉 430081;

²武汉科技大学省部共建耐火材料冶金国家重点实验室, 湖北 武汉 430081

摘要 为了解决常见吸波材料厚度大、吸波频带窄的问题,设计了一种采用新型偶极子方环交叉元结构的带宽大、厚度薄的吸波器,它由导电浆料和氧化铝陶瓷组成。基于有限差分频域方法采用 CST 软件仿真计算了该吸波器的电磁参数与反射率之间的关系。利用等效介质理论反演得到了吸波器的等效电磁参数与等效阻抗。通过优化偶极子方环交叉元结构的单元尺寸和电路参数,设计的吸波器在 11.0~18.0 GHz 频率范围内反射率小于 -10 dB,厚度为 1.6 mm,品质因素(FOM)远高于大多数文献报道的吸波器。研究发现该吸波器的损耗机制为共振损耗和欧姆损耗,组合频率选择表面(FSS)可以增强电磁损耗。实测结果与仿真吻合得较好,该超材料吸波器具有超薄宽带吸收的特性。

关键词 光学设计; 偶极子方环交叉元; 频率选择表面; 等效介质; 电磁损耗

中图分类号 TN928

文献标志码 A

DOI: 10.3788/AOS221446

1 引言

超材料是人造材料,具有天然材料所没有的特殊物理特性,如负折射、负磁导率和负介电常数^[1-3]。通过设计单元的结构、排布方式就能够实现对电磁波的频率、极化、幅度和相位等特性的灵活调控^[4-8]。Veselago最先提出了同时存在负介电常数和负磁导率的假设,并将该介质命名为左手材料,这一结论引起了一系列异常的电磁波传播现象^[9-11]。Pendry成功地通过实验获得了微波波段中金属棒周期阵列和裂环谐振器的有效负介电常数和磁导率,推动了超材料的发展^[12-14]。Smith在Pendry的研究基础上通过将金属丝和谐振环阵列进行合理的排列组合,得到了介电常数和磁导率同时为负的材料,掀起了一股研究电磁超材料的热潮^[15-16]。Landy等^[17-19]提出了第一个完美的超材料吸波器,超材料吸波器比传统的吸波器更有优势,如体积小、厚度薄和设计灵活等。

目前,为了提高超材料吸波器共振频率的数量和强度以增加带宽和降低厚度,采用组合频率选择表面(FSS)来设计超材料吸波器,如双方环路单元、十字方环单元和耶路撒冷十字单元等^[20]。Chen等^[21]对双箭头结构的超材料吸波器进行了研究,其相对带宽为 49.1%,厚度为 2 mm,品质因素(FOM)为 6.8。Jia

等^[22]提出了一种具有正方形和 I 形小块组合结构的超材料吸波器,其相对带宽为 97.9%,厚度为 6 mm, FOM 为 7.99。Fang 等^[23]提出了一种具有分裂同心环结构的超材料吸波器,其相对带宽为 69.2%,厚度为 3 mm, FOM 为 8.05。Qiu 等^[24]提出了一种具有 H 形复合结构的超材料吸波器,其相对带宽为 57.6%,厚度为 1.2 mm, FOM 为 6.68。上述研究为基于组合 FSS 设计薄宽频吸波器提供了指导^[25-26]。

本文采用组合 FSS 来设计薄宽频超材料吸波器,设计了偶极子方环交叉元结构。采用导电浆料和氧化铝陶瓷分别作为 FSS 原料和介质层。对比了偶极子方环交叉元结构和传统方环交叉元结构的吸波效果,由于偶极子方环交叉元结构增强了欧姆损耗,故其吸波效果更好。利用等效介质理论反演得到了等效电磁参数和等效阻抗。值得注意的是,本研究设计的宽频超材料吸波器的厚度远小于目前报道的大多数吸波器。

2 理论模型与仿真

2.1 软件仿真设置

本文使用 CST MICROWAVE STUDIO (CST) 软件进行仿真。由于一维横电磁(TEM)波沿 y 方向传播,故电磁波在 z 方向上的电场分量只有 E_z ,在 x 方

收稿日期: 2022-07-08; 修回日期: 2022-07-21; 录用日期: 2022-08-10; 网络首发日期: 2022-08-20

基金项目: 国家自然科学基金(51972242)

通信作者: *yangxianzhao@wust.edu.cn; **lixiangcheng@wust.edu.cn

向上的磁场分量只有 H_x , 此时麦克斯韦方程^[13]可以写成

$$\begin{cases} \frac{\partial E_z}{\partial t} = \frac{1}{\epsilon} \frac{\partial H_x}{\partial y} \\ \frac{\partial H_x}{\partial t} = -\frac{1}{\mu} \frac{\partial E_z}{\partial y} \end{cases}, \quad (1)$$

式中: ϵ 为介电常数; μ 为磁导率。将该微分方程写成差分形式^[13]可以得到

$$\begin{cases} \frac{E_z^{(n+1/2)}(k) - E_z^{(n-1/2)}(k)}{\Delta t} = \frac{1}{\epsilon} \frac{H_x^{(n)}(k+1/2) - H_x^{(n)}(k-1/2)}{\Delta y} \\ \frac{H_x^{(n+1)}(k+1/2) - H_x^{(n)}(k+1/2)}{\Delta t} = -\frac{1}{\mu} \frac{E_z^{(n+1/2)}(k+1) - E_z^{(n+1/2)}(k)}{\Delta y} \end{cases}, \quad (2)$$

式中: n 为时间离散化步数, 即时间为 $t = \Delta t \cdot n$; k 为空间离散化步数, 即空间距离为 $y = \Delta y \cdot k$; $H(k-1/2)$ 和 $H(k+1/2)$ 为电场 $E(k)$ 附近的磁场值。对式(2)进行变形, 选取合适的时空步长 Δt 和 Δy , 编程写出式(2)在时域的迭代关系。通过激励源的选择和边界条件的确定实现有限差分域法的基本原理。FSS 一般关注整个 S 参数, 即输入反射系数 S_{11} 、反向传输系数 S_{12} 、正向传输系数 S_{21} 和输出反射系数 S_{22} 。CST 的边界条件设置如图 1 所示。

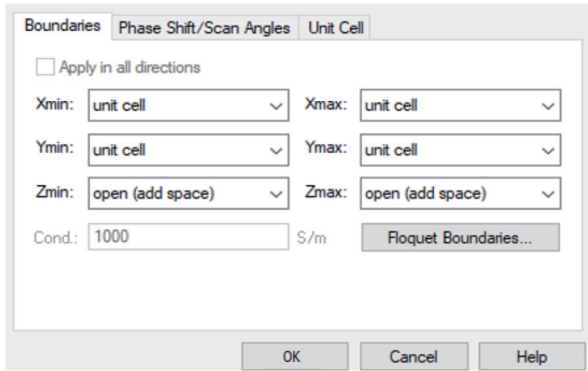


图 1 CST 的边界条件设置

Fig. 1 Boundary condition setting for CST

2.2 吸波器模型和等效电路原理

图 2 显示了所提吸波器的结构和等效电路模型。所提吸波体由损耗层和介质层组成, 损耗 FSS 由丝网印刷将导电油墨印刷在氧化铝介质层(介电常数为 $\epsilon = 9.4$, $\tan \delta = 0.0004$, 其中 δ 为介质损耗角)上得到, 导电油墨的电导率为 24.68 S/m , 介质层厚度 h 为 1.6 mm 。吸收器的底部是金属地面, 可以防止电磁波的传播。

基于等效电路原理, 吸波器上层和底层都相当于输电线路, 可以等效于 RLC 串联电路, 如图 2(b) 所示。吸波器反射率^[13]为

$$r = 20 \lg \left| \frac{Z_{in} - Z_0}{Z_{in} + Z_0} \right|, \quad (3)$$

式中: Z_0 为空气阻抗; 输入阻抗 Z_{in} 等于介质阻抗 Z_{sub} 和表面阻抗 Z_{FSS} 之间的并联组合^[13], Z_{in} 和 Z_{sub} 的表达式为

$$Z_{in} = \frac{Z_{FSS} Z_{sub}}{Z_{FSS} + Z_{sub}}, \quad (4)$$

$$Z_{sub} = Z_0 \cdot \sqrt{1/\epsilon_1} \cdot \tanh \left\{ j(2\pi fh/c) \cdot \sqrt{\epsilon_1} \right\}, \quad (5)$$

式中: ϵ_1 是介质基板的介电常数; f 是微波频率; Z_0 是空气的阻抗; c 是光速。利用遗传算法得到集总元件的优化电路参数, 即电感为 $L = 1.2 \text{ nH}$, 电容为 $C = 0.055 \text{ pF}$

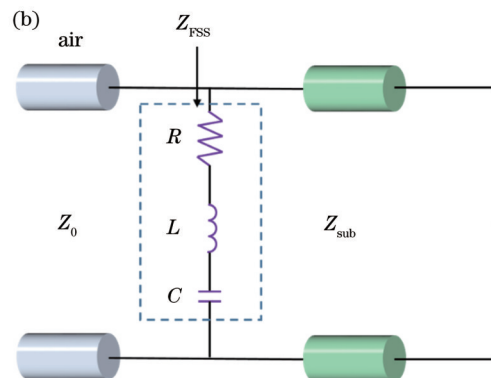
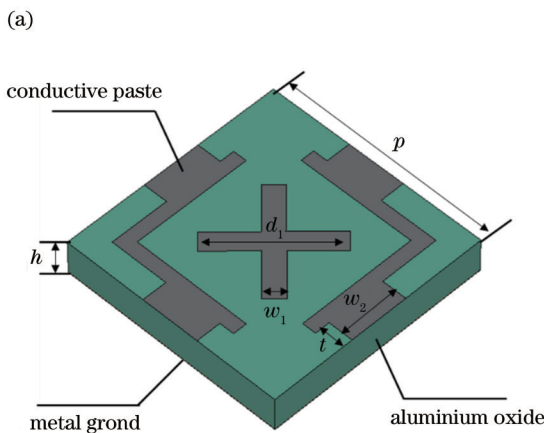


图 2 超材料吸波器的结构示意图和等效电路图。(a)结构示意图;(b)等效电路图

Fig. 2 Structural diagram and equivalent circuit diagram of metamaterial absorber. (a) Structural diagram; (b) equivalent circuit diagram

和电阻为 $R=92 \Omega$ 。在得到电路参数后,可以进一步考虑吸波器单元电池的尺寸。在电路模型中,电感 L 和电容 C 与 FSS 的边长 d 、宽度 w 和周期 p 的关系^[13]为

$$\frac{\omega_r C}{Y_0} = \frac{d}{p} \sec \theta \cdot \frac{p}{\lambda} \ln \left[\csc \left(\frac{\pi g}{2p} \right) \right], \quad (6)$$

$$\frac{\omega_r L}{Z_0} = \frac{d}{p} \cos \theta \cdot \frac{p}{\lambda} \ln \left[\csc \left(\frac{\pi w}{2p} \right) \right], \quad (7)$$

式中: $\omega_r=1/\sqrt{LC}$; $g=d-w$; Y_0 为自由空间导纳; θ 为入射角。超表面结构的最终尺寸为 $p=11.5 \text{ mm}$ 、 $d=10.0 \text{ mm}$ 、 $d_1=4 \text{ mm}$ 、 $w=0.2 \text{ mm}$ 、 $w_1=0.3 \text{ mm}$ 和 $w_2=0.7 \text{ mm}$ 。

2.3 仿真结果对比

为了研究 FSS 对吸波效果的影响,设计了三种不同的 FSS。为了便于区分,将其分别命名为结构 A、结构 B 和结构 C,如图 3 所示。

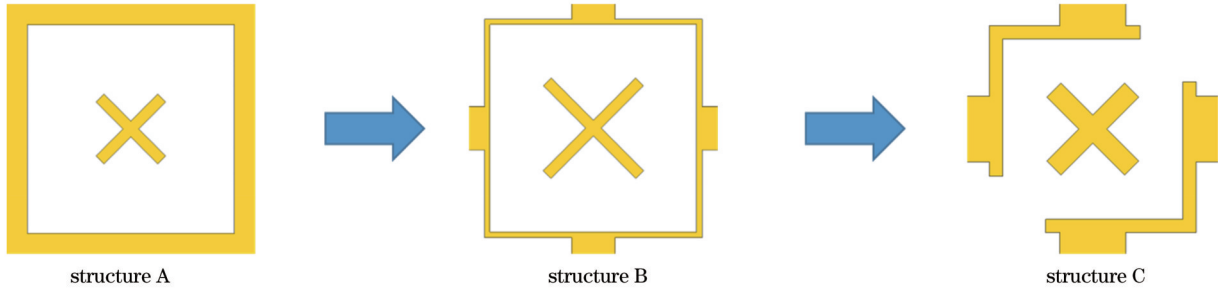


图 3 三种不同 FSS 的结构示意图

Fig. 3 Structural diagrams of three different FSSs

图 4 是结构 A 吸波器、结构 B 吸波器和结构 C 吸波器根据方程(1)和方程(2),通过 CST 计算得到的反射系数。结构 A (方环交叉元) 可以实现在 12.2~13.8 GHz 频率范围内反射率小于 -10 dB, 吸收峰在

13.0 GHz 处, 吸收强度可达到 -25 dB。在结构 A 的基础上, 增加了 T 形节点设计了结构 B (T 形方环交叉元), 结构 B 可以实现在 11.7~14.0 GHz 频率范围内反射率小于 -10 dB, 吸收峰移动至 12.5 GHz 处, 吸收强度降低至 -19 dB。可以发现, 虽然引入 T 形节点可以扩大带宽, 但是会导致吸收峰处的吸收强度降低。为了进一步扩大带宽和提高吸收强度, 通过引入缺口方环设计了结构 C (偶极子方环交叉元), 结构 C 可以实现在 11.0~18.0 GHz 频率范围内反射率小于 -10 dB, 吸收峰在 12.7 GHz 处, 吸收强度可达到 -29 dB。可以发现, 偶极子的引入使得带宽和吸收强度都有了明显的提升。因此, 采用结构 C 设计吸波器可以增加带宽和减小厚度。

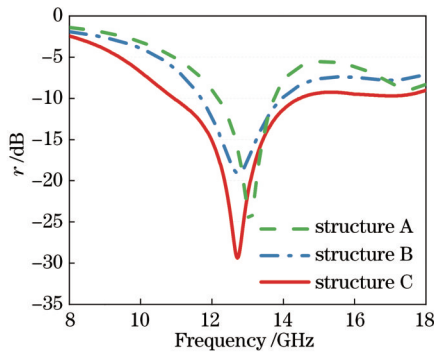


图 4 三种不同结构 FSS 的反射系数

Fig. 4 Reflection coefficients of FSSs with three different structures

在结构参数中, 介质基板的厚度和吸波器的表面电阻是影响反射率的两个重要因素, 研究了这两个因素对超材料吸波器性能的影响, 如图 5 所示。

图 5(a) 为不同厚度下的仿真结果。可以发现, 当

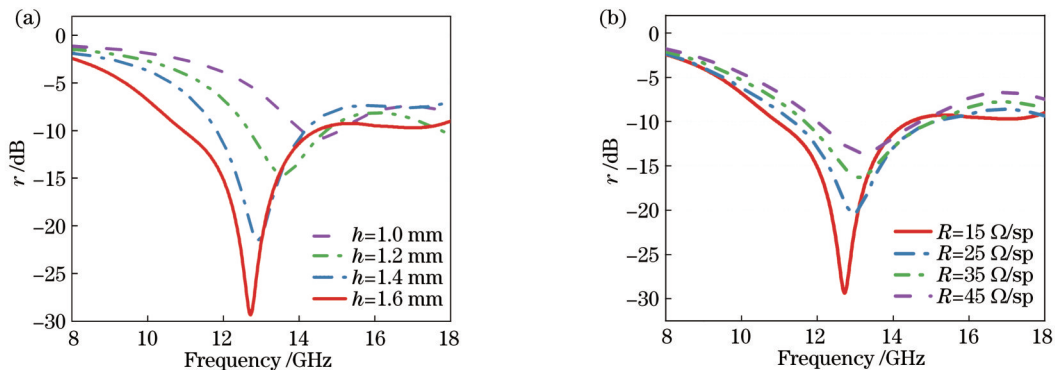


图 5 不同参数下超材料吸波器的反射率曲线。(a) h ; (b) R

Fig. 5 Reflectivity curves of metamaterial absorber under with different parameters. (a) h ; (b) R

厚度从 1.6 mm 减小到 1.0 mm 时,吸波器的整体吸收带宽向高频移动,共振频率也由 12.8 GHz 移动到 14.0 GHz,最小反射率值从 -29.0 dB 降低到 -11.2 dB。电磁波进入氧化铝涂层后,随着厚度的减小,电磁波更难在其中被消耗完,故超材料吸波器的吸波效果会变差。在 Rozanov 的研究中发现,吸波器的厚度并不是可以无限减小的,厚度带宽比有一个下界。

图 5(b) 为不同表面电阻下的仿真结果。可以发现,当表面电阻从 15 Ω/sp 增大到 45 Ω/sp 时,最小反射率值从 -29 dB 降低到 -13 dB,吸收带宽也明显降低。模拟结果表明,最佳的表面电阻会使超材料吸波器的吸波系数达到最大和吸收带达到最宽。这表明超材料吸波器的吸波率大小取决于单元结构的几何参数和 FSS 的方阻值能否进行良好的阻抗匹配。

图 6 为所设计吸波器在横电 (TE) 和横磁 (TM) 偏振模式下不同斜入射角时的反射率性能。可以发现,当入射角大于 20° 时,反射率开始降低,这是由偶极子方环交叉单元的周期比工作波长大造成的。

3 结果与讨论

3.1 吸波器等效介质分析

为了更准确地分析结构的吸收机理,采用了等效介质模型,如图 7 所示,其中 E_1^i 为空气中的入射波、 E_1^r 为空气中的反射波、 E_2^i 为介质中的入射波、 E_2^r 为介质中的反射波。

通过反射系数和透射系数的散射参数反演等效电

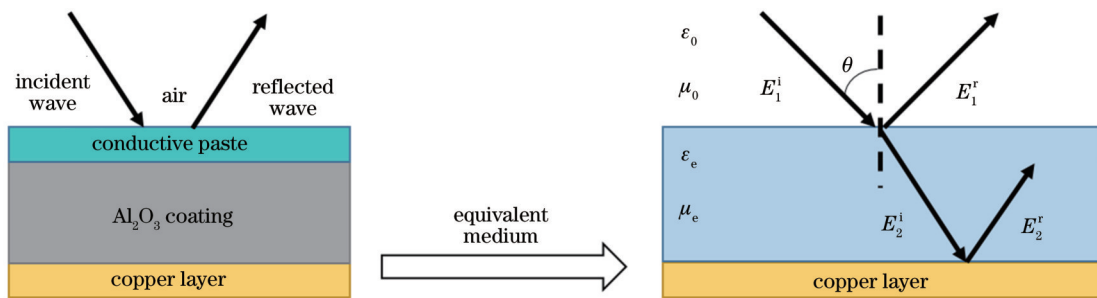


图 7 等效介质模型

Fig. 7 Equivalent medium model

将组合设计得到的 FSS 超材料吸波器等效为具有相同厚度的均匀材料,并利用 S 参数反演得到等效电磁参数,对应的等效介电常数、等效磁导率,以及等效阻抗的实部和虚部如图 8 所示。由图 8(a)、(b) 可以看到,在 12.7 GHz 处介电常数的实部与磁导率实部相等,介电常数的虚部与磁导率虚部相等,这说明该频率是共振频率。由图 8(c) 可以看到,在 12.7 GHz 处归一化阻抗实部接近于 1,虚部接近于 0,这说明在 12.7 GHz 处吸波器的阻抗和空气阻抗匹配得较好,吸收效果接近完美。由此可见,12.7 GHz 处的吸收机制

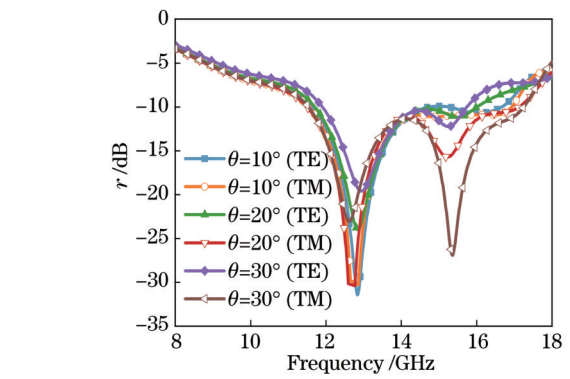


图 6 所设计吸波器在 TE 和 TM 偏振模式下不同斜入射角时的反射率

Fig. 6 Reflectivity of designed absorber for different oblique incidence angles in TE and TM polarization modes

磁参数,等效阻抗 (Z_e) 和等效折射率 (n_e) 的表达式为

$$Z_e = \pm \sqrt{\frac{(1 + S_{11})^2 - S_{21}^2}{(1 - S_{11})^2 - S_{21}^2}}, \quad (8)$$

$$n_e = \frac{1}{k_0 h} \left\{ \left\{ \ln \left[\exp(j2nk_0 h) \right] \right\}'' + 2m\pi - j \left\{ \ln \left[\exp(j2nk_0 h) \right] \right\}' \right\}, \quad m = 1, 2, 3, \dots, \quad (9)$$

等效介电常数和等效磁导率的表达式为

$$\epsilon_e = n_e / Z_e, \quad (10)$$

$$\mu_e = n_e \cdot Z_e, \quad (11)$$

式中: Z_e 为相对阻抗; n 为折射率; k_0 为自由空间入射波数。

是磁共振。

3.2 吸波器电磁损耗分析

为了探明超材料的吸收增强机理,研究了吸波器在共振频率 12.7 GHz 处的表面电流方向,如图 9 所示。图 9 描绘了谐振频率处超材料吸波器表面电流的流动示意图,当横向电场沿 x 轴入射到超材料吸波器上时,顶部产生了电流。感生的交变电流将产生交变磁场,顶部的感应电流产生的感应磁场会进一步在氧化铝涂层上产生一个电场,驱动着反射底板的电流沿着与顶部感应电流相反的方向运动,两者之间形成一

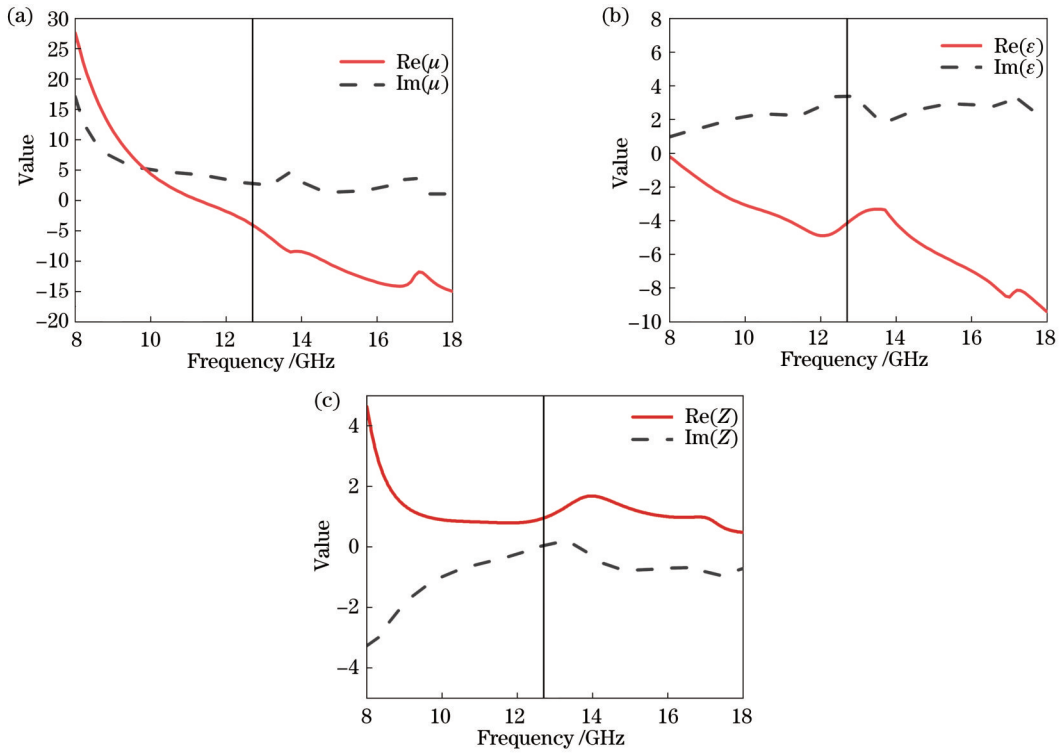


图 8 等效电磁参数。(a) 等效介电常数; (b) 等效磁导率; (c) 等效阻抗

Fig. 8 Equivalent electromagnetic parameters. (a) Equivalent permittivity; (b) equivalent permeability; (c) equivalent impedance

个闭环回路,如图 9(c)所示。同时, 交变磁场产生交变电场会引起表面电流的显著增加, 表面电流的增强改善了表面功率损耗。由于 FSS 层存在电阻, 故高密

度的表面电流会造成欧姆损耗, 这是 12.7 GHz 处吸收良好的主要原因。模拟结果表明, 超材料涂层表面与底部金属板在吸收峰频率处产生了明显的近场耦合。

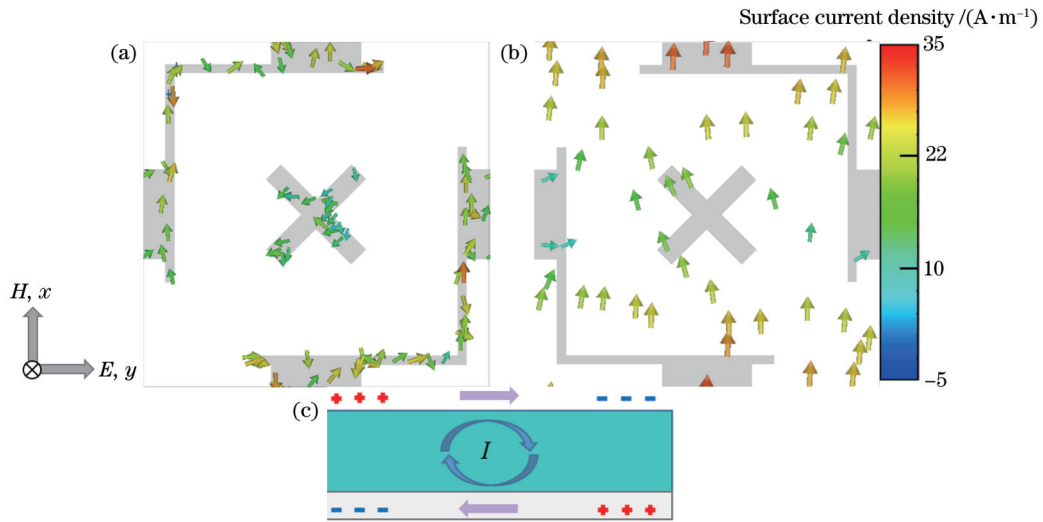


图 9 吸波器在共振频率的电流分布。(a) FSS 的表面电流; (b) 介质背板的表面电流; (c) 磁谐振时表面电流的流动

Fig. 9 Current distribution of absorber at resonant frequency. (a) Surface current of FSS; (b) surface current of dielectric backplane; (c) surface current flow during magnetic resonance

图 10 为超材料吸波器在吸收峰频率处的功率损耗密度分布, 还对吸收峰频率处的电场进行了监测。可以发现, 磁谐振电路增强了超材料涂层表面的电场。另外, 损耗介质对电磁能量的吸收^[12-13]可以描述为

$$P_{\text{abs}} = \frac{\omega \operatorname{Re}(\epsilon) + \sigma}{2} \times |E|^2, \quad (12)$$

式中: ω 为角频率; $\operatorname{Re}(\epsilon)$ 为介电常数的实部; E 为总电场强度; σ 为损耗介质的电导率; P_{abs} 为电磁吸收功率。由式(12)可知, 随着 E 的增大, 超材料吸波器吸收性能

也会相应提高。

由图 10(a)、(b)可以看出,结构 A 的功率损耗密度分布主要集中在交叉元中心和方环的两个导电带上,由于元素的对称性,TE 极化和 TM 极化的功率损耗分布是一致的。由图 10(c)、(d)可以看出,结构 B 的功率损耗密度分布主要集中在交叉元中心和 T 形结点周围,由于引入 T 形结点会引起电子聚集,故方环上功率损耗密度出现了明显的强弱区间,而不是像结构 A

那样在方环上均匀分布。图 10(e)、(f)可以看出,与结构 B 相比,结构 C 中缺口的出现使得上下两处 T 形结点的功率损耗显著增加,左右两处 T 形结点的功率损耗显著降低。这是因为缺口的存在导致电流无法流通,正负电子分别聚集在缺口两侧形成偶极子,偶极子产生强烈的电场。在电场增强区域中,入射电磁波的能量损失明显增加,故采用结构 C 设计吸波器可以增加带宽和减小厚度。

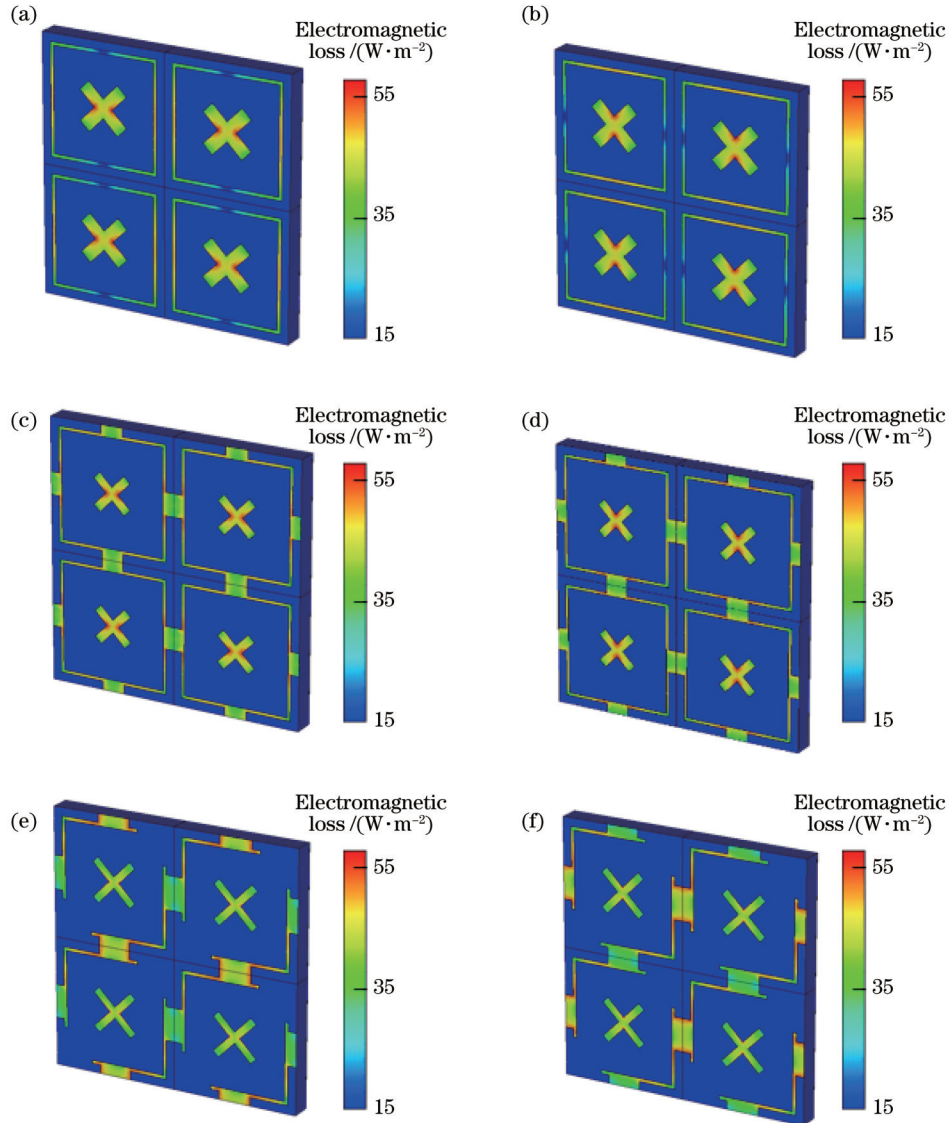


图 10 12.7 GHz 吸收峰处的电磁损耗。(a)方环交叉元 TE 模式;(b)方环交叉元 TM 模式;(c) T 形方环交叉元 TE 模式;(d) T 形方环交叉元 TM 模式;(e)缺口 T 形方环交叉元 TE 模式;(f)缺口 T 形方环交叉元 TM 模式

Fig. 10 Electromagnetic loss at 12.7 GHz absorption peak. (a) TE mode of square ring crossed element; (b) TM mode of square ring crossed element; (c) TE mode of T-shaped square ring crossed element; (d) TM mode of T-shaped square ring crossed element; (e) TE mode of notched T-shaped square ring crossed element; (f) TM mode of notched T-shaped square ring crossed element

3.3 实验验证

根据 Rozanov 极限定律,吸波器的厚度和吸波带宽存在着制约关系,吸波器的极限厚度带宽比公式^[8]为

$$|\ln \rho_0|(\lambda_{\max} - \lambda_{\min}) < 2\pi^2 \sum_i \mu_{s,i} h_i, \quad (13)$$

式中: λ_{\max} 和 λ_{\min} 分别为工作频率下自由空间波长的最大值和最小值; ρ_0 为反射系数;对于非磁性吸波器, $\mu_{s,i}=1$; h_i 为吸波器厚度。为了评估厚度与频宽的综合

性能,采取品质因素(FOM)对吸波器的性能进行评估^[23],其表达式为

$$V_{\text{FOM}} = \frac{\Delta f C_0}{h f_L f_0}, \quad (14)$$

式中: Δf 为带宽; C_0 为自由空间中的光速; f_L 为反射率

的最低频率; f_0 为反射率的中心频率。图 11 为设计吸波器实物图和模拟与测试的结果。表 1 将所设计吸波器的 FOM 与其他文献报道的吸波器进行了比较。可以发现,本文样品的 FOM 比表中其他样品都要大,这在实际应用中有重要意义。

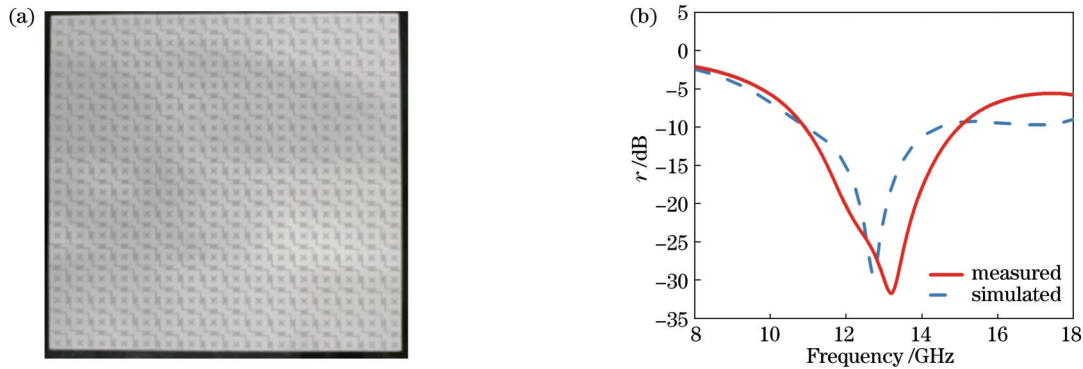





图 11 所设计吸波器的实物图和模拟与测试的结果。(a) 实物图;(b)模拟与测试结果

Fig. 11 Actual picture and measured and simulated results of designed absorber. (a) Actual picture; (b) measured and simulated results

表 1 所设计吸波器与其他文献报道的吸波器性能的比较

Table 1 Performance comparison of designed absorber in this paper with those reported in other literatures

Ref.	-10 dB bandwidth	Thickness /mm	Relative bandwidth /%	FOM	FSS
[21]	6.1-17.8	6.0	97.9	7.99	
[22]	10.6-17.5	2.0	49.1	6.80	
[23]	8.6-17.7	3.0	69.2	8.05	
[24]	21.0-38.0	1.2	57.6	6.86	
Our work	11.0-18.0	1.6	62.6	9.39	

4 结 论

基于偶极子方环交叉元结构设计并制作了一款带宽大、厚度薄的超材料吸波器。利用 CST 软件基于时域有限积分求解三种基于交叉元结构的超材料吸波器的反射率,研究了超表面结构对反射率的影响。通过在共振频率处的表面电流分布和电磁损耗密度分析了该吸波器的吸波损耗机理,即缺口的存在导致电流无法流通,正负电子分别聚集在缺口两侧形成偶极子,偶极子产生强烈的电场,在电场增强区域中入射电磁波的能量被快速损耗。同时,利用等效介质理论反演得到了吸波器的等效介电常数、等效磁导率和等效阻抗,研究发现该超材料吸波器的损耗机制为磁谐振激发。仿真和实验结果吻合得较好,实验结果与仿真结果有少量偏差是由仿真模型无限大且具有理想边界条件造

成的。超材料吸波器在 11.0~18.0 GHz 波段的反射率小于 -10 dB,12.7 GHz 处微波吸收率达到最大值,厚度为 1.6 mm。本研究生产原材料的简单性和超材料吸波器制作的可行性让该吸波器的大规模应用成为可能。

参 考 文 献

- [1] Kim Y, Deng T W, Jiang W X, et al. Robust control of a multifrequency metamaterial cloak featuring intrinsic harmonic selection[J]. *Physical Review Applied*, 2018, 10(4): 044027.
- [2] Kadic M, Bückmann T, Schittny R, et al. Metamaterials beyond electromagnetism[J]. *Reports on Progress in Physics*, 2013, 76(12): 126501.
- [3] Alekseev G V, Tereshko D A. Particle swarm optimization-based algorithms for solving inverse problems of designing thermal cloaking and shielding devices[J]. *International Journal of Heat and Mass Transfer*, 2019, 135: 1269-1277.
- [4] Henriquez V C, Garcia-Chocano V M, Sánchez-Dehesa J.

- Viscothermal losses in double-negative acoustic metamaterials [J]. *Physical Review Applied*, 2017, 8(1): 014029.
- [5] Chen T Y, Weng C N, Tsai Y L. Materials with constant anisotropic conductivity as a thermal cloak or concentrator[J]. *Journal of Applied Physics*, 2015, 117(5): 054904.
- [6] Dede E M, Nomura T, Lee J. Thermal-composite design optimization for heat flux shielding, focusing, and reversal[J]. *Structural and Multidisciplinary Optimization*, 2014, 49(1): 59-68.
- [7] Li W W, Chen M J, Zeng Z H, et al. Broadband composite radar absorbing structures with resistive frequency selective surface: optimal design, manufacturing and characterization[J]. *Composites Science and Technology*, 2017, 145: 10-14.
- [8] Rozanov K N. Ultimate thickness to bandwidth ratio of radar absorbers[J]. *IEEE Transactions on Antennas and Propagation*, 2000, 48(8): 1230-1234.
- [9] 杨洁萍, 王民昌, 邓琥, 等. 超材料吸收器集成微流控的双带太赫兹传感器[J]. *光学学报*, 2021, 41(23): 2328001.
Yang J P, Wang M C, Deng H, et al. Dual-band terahertz sensor based on metamaterial absorber integrated microfluidic[J]. *Acta Optica Sinica*, 2021, 41(23): 2328001.
- [10] Deng Y D, Song Z Y. Manipulating polarization and electromagnetically induced transparency in a switchable metamaterial[J]. *Optical Materials*, 2020, 105: 109972.
- [11] Kundtz N, Smith D R. Extreme-angle broadband metamaterial lens[J]. *Nature Materials*, 2010, 9(2): 129-132.
- [12] Qu S C, Sheng P. Microwave and acoustic absorption metamaterials[J]. *Physical Review Applied*, 2022, 17(4): 047001.
- [13] Zheng L, Yang X Z, Gong W, et al. Ultralow thickness-bandwidth ratio magnetic absorber with printed FSS for S&C bands[J]. *IEEE Antennas and Wireless Propagation Letters*, 2022, 21(3): 576-580.
- [14] 孙树林, 何琼, 郝加明, 等. 超构表面高效调控电磁波[J]. *光学学报*, 2021, 41(1): 0123003.
Sun S L, He Q, Hao J M, et al. High-efficiency manipulations on electromagnetic waves with metasurfaces[J]. *Acta Optica Sinica*, 2021, 41(1): 0123003.
- [15] Chen C X, Can S, Schalch J, et al. Ultrathin terahertz triple-band metamaterial absorbers: consideration of interlayer coupling [J]. *Physical Review Applied*, 2020, 14(5): 054021.
- [16] Bharti G, Jha K R, Singh G. A synthesis technique of single square loop frequency selective surface at terahertz frequency[J]. *Optik*, 2014, 125(21): 6428-6435.
- [17] Landy N I, Sajuyigbe S, Mock J J, et al. Perfect metamaterial absorber[J]. *Physical Review Letters*, 2008, 100(20): 207402.
- [18] 刘艳红, 任咪娜, 董丽娟, 等. 平坦等频面双曲超材料的奇特电磁传输性[J]. *光学学报*, 2022, 42(2): 0216001.
Liu Y H, Ren M N, Dong L J, et al. Novel electromagnetic propagation in hyperbolic metamaterials with flat iso-frequency planes[J]. *Acta Optica Sinica*, 2022, 42(2): 0216001.
- [19] Xu L J, Huang J P. Metamaterials for manipulating thermal radiation: transparency, cloak, and expander[J]. *Physical Review Applied*, 2019, 12(4): 044048.
- [20] Deng G S, Sun H X, Lü K, et al. Enhanced broadband absorption with a twisted multilayer metal-dielectric stacking metamaterial[J]. *Nanoscale Advances*, 2021, 3(16): 4804-4809.
- [21] Chen H Y, Wang J F, Ma H, et al. Ultra-wideband polarization conversion metasurfaces based on multiple plasmon resonances [J]. *Journal of Applied Physics*, 2014, 115(15): 154504.
- [22] Jia Y T, Liu Y, Guo Y, et al. A dual-patch polarization rotation reflective surface and its application to ultra-wideband RCS reduction[J]. *IEEE Transactions on Antennas and Propagation*, 2017, 65(6): 3291-3295.
- [23] Fang W, Fan D G, Xie X Y, et al. A broadband radar cross section reduction metasurface based on polarization conversion and scattering cancellation[C]//2019 Cross Strait Quad-Regional Radio Science and Wireless Technology Conference (CSQRWC), July 18-21, 2019, Taiyuan, China. New York: IEEE Press, 2019.
- [24] Qiu L N, Xiao G B, Kong X H, et al. Broadband, polarization insensitive low-scattering metasurface based on lossy Pancharatnam-Berry phase particles[J]. *Optics Express*, 2019, 27(15): 21226-21238.
- [25] 王岩, 陈哲, 崔琦. 基于二氧化钒的可调谐太赫兹宽带带通滤波器[J]. *光学学报*, 2021, 41(20): 2023002.
Wang Y, Chen Z, Cui Q. Tunable terahertz broadband bandpass filter based on vanadium dioxide[J]. *Acta Optica Sinica*, 2021, 41(20): 2023002.
- [26] Yang L J, Lü H L, Li M, et al. Multiple polarization effect of shell evolution on hierarchical hollow C@MnO₂ composites and their wideband electromagnetic wave absorption properties[J]. *Chemical Engineering Journal*, 2020, 392: 123666.

Design of Thin Wideband Absorber Based on Lossy Capacitive Surface of Dipole Square Ring Crossed Element

Lin Yifu^{1,2}, Yang Xianzhao^{1*}, Li Xiangcheng^{2**}

¹*Engineering Research Center for Metallurgical Automation and Measurement Technology of Ministry of Education, Wuhan University of Science and Technology, Wuhan 430081, Hubei, China;*

²*State Key Laboratory of Refractories and Metallurgy, Wuhan University of Science and Technology, Wuhan 430081, Hubei, China*

Abstract

Objective With the development of information technology, electronic devices are widely used while leading to many electromagnetic interference problems. In addition, useless electromagnetic waves may pose a potential threat to human health. Therefore, electromagnetic absorbing materials have been developed to eliminate electromagnetic interference and provide information security. Conventional coated absorbing materials usually have a narrow and fixed absorbing band and

are susceptible to external environmental influences. Compared with traditional absorbers, metamaterial absorbers have a larger absorbing bandwidth, a stronger absorbing capacity, and a lower thickness. To solve the problem that common absorbing materials have a high thickness and a narrow absorption band, a new dipole square ring crossed element structure with a large bandwidth and a low thickness is designed in this paper. This new structure shows good stability and high-frequency characteristics.

Methods In this paper, the relationship between the electromagnetic parameters and the reflectivity of the absorber is calculated by the finite-difference time-domain method through simulation with CST software. The equivalent electromagnetic parameters of the absorber are obtained by inversion according to the equivalent medium theory. The cell size and circuit parameters of the dipole square ring crossed element structure are optimized by the equivalent circuit model of the absorber. The influence of two main parameters on reflectivity is studied. The surface current, electric energy density, and magnetic energy density of a unit cell at the operating frequency are simulated to analyze the working mechanism. A high-impedance surface comprising a lossy frequency selective surface (FSS) is employed to design a broadband microwave metamaterial absorber. The dipole square ring cross element structure is designed. Conductive paste and alumina ceramic are selected as the FSS raw material and the dielectric layer, respectively. Firstly, the alumina ceramic is used to make the dielectric substrate so that the limit thickness can be reduced. Secondly, the conductive paste is applied to the dielectric layer by the screen printing method, and the surface square resistance of the conductive paste is $60 \Omega/\text{sp}$. Finally, the reflection coefficient of the sample is measured by the free-space method in a microwave darkroom with a double-ridged horn antenna and a network analyzer.

Results and Discussions The metamaterial absorber has a reflectivity less than -10 dB in the frequency range of 11.0–18.0 GHz, a thickness of 1.6 mm, and a much higher figure of merit (FOM) than most reported absorbers. Three different FSSs are designed for comparison, and the dipole square ring cross element structure possesses a larger bandwidth and a stronger absorption effect. Surface current and electromagnetic power loss density are analyzed (Fig. 10). Because the current cannot flow due to the gaps, positive and negative electrons gather on the two sides of the gaps respectively to form dipoles which can generate a strong electric field. In the electric field enhancement region, the energy loss of the incident electromagnetic wave increases significantly. Therefore, the dipole square ring cross element structure is used to design an absorber with an increased bandwidth and a reduced thickness. The effects of the thickness of the dielectric substrate and the surface resistance of the absorber on the reflectivity are investigated (Fig. 5). After the electromagnetic wave enters the alumina coating, its consumption becomes more difficult as the thickness decreases, so the absorption of the metamaterial absorber becomes less effective. The simulation results show that the optimal surface resistance results in the largest absorption coefficient and the widest absorption band of the metamaterial absorber.

Conclusions In this paper, a thin wideband metamaterial absorber is designed and fabricated with a dipole square ring cross element structure. The reflectivities of three metamaterial absorbers based on cross element structures are solved using CST software through time-domain finite integration, and the effect of the metasurface structure on the reflectivity is investigated. According to the analysis of the surface current distribution and electromagnetic loss density at the resonance frequency, the absorbing loss mechanism is made clear, namely that the existence of the gaps makes the current fail to flow, and positive and negative electrons gather on the two sides of the gaps respectively to form dipoles able to generate a strong electric field. The energy of the incident electromagnetic wave is rapidly lost in the electric field enhancement region. The equivalent dielectric constant, equivalent permeability, and equivalent impedance of the absorber are obtained by inversion in light of the equivalent medium theory, and it is found that the loss mechanism of the metamaterial absorber is the excitation of magnetic resonance. The simulation and experimental results are in good agreement. The experimental results have a small deviation from the simulation results because the simulation model is an infinite one and has ideal boundary conditions. The metamaterial absorber has a reflectivity less than -10 dB in the 11.0–18.0 GHz band with a thickness of 1.6 mm, and the microwave absorption peaks at 12.7 GHz. The simplicity of the raw materials produced in this study and the feasibility of the metamaterial absorber fabrication make the large-scale application of the designed absorber possible.

Key words optical design; dipole square ring crossed element; frequency selective surface; equivalent medium; electromagnetic loss